GEOLOGICA CARPATHICA, DECEMBER 2020, 71, 6, 503–515 https://doi.org/10.31577/GeolCarp.71.6.2

Cyclicity of Middle Jurassic calciturbidites of the Travnik Formation, Bovec Basin, NW Slovenia

ANDREJ ŠMUC[1,✉], BOŠTJAN ROŽIČ[1] and TIMOTEJ VERBOVŠEK[1]

[1]University of Ljubljana, Faculty of Natural Sciences and Engineering, Department of Geology, Aškerčeva 12, 1000 Ljubljana, Slovenia; ✉andrej.smuc@geo.ntf.uni-lj.si

(Manuscript received March 23, 2020; accepted in revised form December 9, 2020; Associate Editor: Jozef Michalík)

Abstract: We investigate calciturbidite cyclicity using statistical method based on time-series analysis (Fourier analysis) of bed thickness patterns. This method was applied to four members of the Jurassic calciturbidite-dominated Travnik Formation of the Bovec Trough outcropping in three adjacent and correlated sections. Our study has shown that the Fourier analysis of calciturbidite bed thicknesses is not successful for reconstruction of cyclicity in erosional upper slope depositional environments (Member 3). On the contrary, the method shows meaningful results for lower slope and distal basin floor depositional setting (Members 1, 2, 4). Here we detected variability of cyclicity in the same time frame of deposition and also subtle lateral variation of the stacking pattern between different sections. Each section contains regional low-frequency cycles common to all sections, and superimposed specific "local" high-frequency cycles. Tectonic factors have an influence on the low frequency, and other factors, such as the local topography, climate, different position on a depositional lobe or magnitude of the turbidite event, can force the high-frequency cycles. We calculated nine cycles for Bajocian and Bathonian (Members 1 and 2), and also nine cycles from Early Callovian to Middle/Late Oxfordian (Member 4). Due to the erosional nature of the Member 3 (Bathonian to Early Callovian) sedimentary environment, reliable comparison to Jurassic sea-level variations was not possible.

Keywords: cyclicity, calciturbidites, Middle Jurassic, Travnik Formation, Bovec Trough, Slovenia.

Introduction

Cyclicity is a common feature of past and recent calciturbidite depositional sequences. The cyclicity is regularly expressed and evaluated as a fluctuation of different calciturbidite parameters including frequency of calciturbidites, variations in bed thickness, grain size, sorting, mineralogy (content of aragonite, calcite, magnesian calcite, dolomite, and quartz), variations in the composition of transported grain (reflecting different source areas like platform interior, shallow, deeper or fore reef settings and open ocean), variations of petrophysical properties (colour, porosity, natural gamma-ray values, bulk density, P-wave velocity values) and geochemistry (δ18O) (Mullins & Cook 1986; Reijmer et al. 1988, 1991, 1994; Haak & Schlager 1989; Eberli 1991; Betzler et al. 1995, 1999, 2000; Satterley 1996; Anselmetti et al. 2000; Bernet et al. 2000; Schwarzacher 2000; Isern & Anselmetti 2001; Blomeier & Reijmer 2002; Rendle & Reijmer 2002; Maurer et al. 2003; Mawson & Tucker 2009).

The distinct stacking pattern of calciturbiditic successions is determined by several autocyclic and allocyclic factors that define not only the sediment production on the carbonate platform, but also the subsequent shedding of excess material from the platform into adjacent basins and other resedimentation processes. These factors act on different time scales, from thousands to millions of years, and include oceanographic variations (salinity, water temperature, turbulence, currents), climatic and relative sea-level changes, platform and slope architecture, regional and local tectonics, biotic composition, and/or lateral migration of sediment bodies (cf. Ferry & Rubino 1987; Eberli 1991; D'Argenio et al. 1999; Bernet et al. 2000; Blomeier & Reijmer 2002; Drzewiecki & Simo 2002; Lantzsch et al. 2007; Bosence et al. 2009; Tresch & Strasser 2011). In a natural carbonate environment, these controlling factors are usually interconnected, some are interdependent and some are not (cf. Nicolis & Nicolis 1991). As a result, calciturbiditic successions sometimes show no apparent cyclicity, or the cycles are obscured by partial overlapping cycles of different length. This can be a problem if the detection of cycles is obtained only visually from lithological, compositional, petrophysical or bed thickness plots, as is usually the case. Such methods may introduce a subjective approach, which may vary from researcher to researcher and may be influenced by her or his experience.

The focus of our work is the investigation of calciturbidite cyclicity using statistical methods based on time-series analysis of bed thickness patterns by Fourier analysis. We used bed thickness parameter for two reasons. First the bed thickness can be quite easily and "relatively" precisely measured. On the other hand, in the Jurassic (especially Early and Middle), due to the scarcity of pelagic carbonate grain producers, the majority of carbonate grains (even fine-grained carbonate fraction) are shed from the adjacent carbonate platforms and transported to the adjacent basins. Therefore, the large majority of the carbonate in the calciturbidite, debrite and also background-hemipelagic beds had shallow-water

origin. However, it should be mentioned that to minor extent also pelagic (filaments) grains are present in the measured beds.

With this method we want to calculate the number of detected cycles in the calciturbidites and intercalated debris and background-hemipelagic beds, determine their intensity and separate cycles with a stronger "signal" from weaker ones. In addition, we decompose and identify individual cycles from a complex superposition of cycles with different wavelengths. These typically occur over time due to cyclical variations in sea level, climate, subsidence patterns, and biological carbonate productivity. These cycles are commonly observed in calciturbidite successions. Their compositional variations have been thoroughly investigated by Haak & Schlager 1989; Everts 1991; Reijmer & Everaars 1991; Reijmer et al. 1991, 1992, 1994, 2012, 2015; Reijmer 1998; Everts et al. 1999; Andresen et al. 2003; Maurer et al. 2003. However, the quantification of the cyclicity itself using statistical methods based on time series analysis (sensu stricto) is still relatively rarely applied to calciturbidites (Roth & Reijmer 2005) compared to siliciclastic systems.

We should remark that "mathematically" defined sedimentological cycles can sometimes be different; compared to visually defined sedimentological cycles. The visual recognition of sedimentological cycles depends on the knowledge of observer, and/or the cycles can be poorly visible due to only subtle variations in given parameters, they can be masked by partial overlap of cycles of different length and so on. Considering the bed thickness, one should note that this parameter can only be approximately measured, and this is accepted if the cycle is sufficiently visually expressed. The recognition of "mathematical" cycles, however, have their basis in the quantitative recognition of whatever process is driving the cycles. These cycles are calculated by several mathematical methods (for example the Fourier method), which are very strict and exact. These cycles are recognized by completely automatic mathematical algorithm, and their recognition is stricter (and consequently sometimes unsuccessful). We have tried to apply the latter method (mathematical), to determine the cycles objectively, and make the interpretation based on geological processes, which of course also drive these cycles. The Fourier method was used, as it is very suitable due to recognition of a complete cycle spectrum of different frequencies at the same time and is therefore appropriate for determination of different cycles in bedded rocks. Our studied cycles are based on the bed thickness analysis, with cyclicity based on the repetition (number of) of similarly thick- or thin-bedded rocks.

These methods were applied to three sections of the Middle to Upper Jurassic Bovec Trough sequence dominated by calciturbidites (Travnik Formation). These three sections represent an ideal location for such an investigation, as they allow the correlation of possible cycles between the sections and the separation of individual "local" and common "regional" cycles.

Geological setting and lithostratigraphy

The successions of the Travnik Formation are located on the Mangart Saddle mountain in the Julian Alps, north-western Slovenia (Fig. 1). They structurally belong to the Julian Nappe in the easternmost part of the Southern Alps (Placer 2008) (Fig. 1). The sediments of the Travnik Fm. were deposited in the Bovec Trough, a small basin that developed in the Early Jurassic as part of the rifted southern passive continental margin of the Tethys (Cousin 1981; Buser 1989; Jurkovšek et al. 1990; Goričan et al. 2003; Šmuc 2005; Šmuc & Goričan 2005; Črne et al. 2007). During the Middle and Late Jurassic, the Bovec Trough was slowly infilled with resedimented shallow-water material from the adjacent, highly productive Dinaric Carbonate Platform. The complex Tertiary polyphase thrusting and Neogene lateral displacement almost completely obliterated the original paleogeographical position of the area. All sections of the Travnik Fm. belong to the same structural subunit (Travnik structural unit in Šmuc 2005) with only slight internal duplex thrusting (Figs. 2, 3).

The Travnik Formation is early-middle Bajocian to early Tithonian in age. The age of the formation and its members was determined with eight samples containing well-preserved radiolarians and using radiolarian Unitary Association Zones (UAZs). The Travnik formation consists of a succession of pelagic background sediments, up to 120 m thick, with intercalated, abundant platform-derived calciturbidites and debris-flow deposits (Fig. 4). The gravity deposits are in places partly or completely silicified by black replacement cherts. The formation is subdivided into four members.

Member 1 (m1) is early-middle Bajocian to late Bajocian in age and was deposited on a complex sea-bottom morphology within a distal basin-floor environment (Šmuc 2005; Šmuc & Goričan 2005). The entire succession is characterized by the occurrence of abundant bedded hemipelagic carbonate mudstones with radiolarians (Figs. 4, 5, 6, 7/1), and fine- to coarse-grained calciturbidites with resedimented ooids and filaments (Fig. 7/2). In condensed successions, m1 is represented by basal carbonate breccias with older lithoclasts that

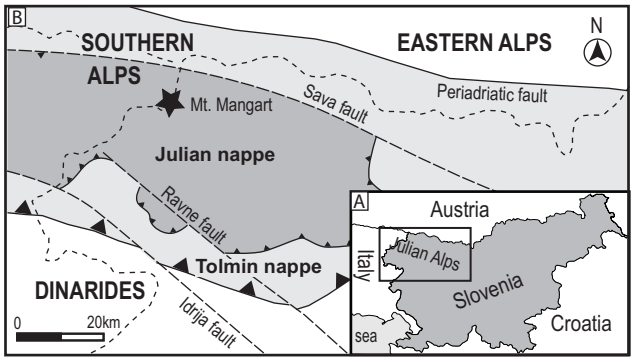

Fig. 1. A — Present location of Julian Alps. **B** — Macrotectonic subdivision of Western Slovenia (modified from Placer 2008) with marked location of the studied area.

grade into fine- to coarse-grained calciturbidites with ooids. Member 2 (m2) is Bathonian in age and the sediments were deposited in a lower slope environment (Šmuc 2005; Šmuc & Goričan 2005). It is represented by thick beds of medium- to coarse-grained calciturbidites (Figs. 4, 6, 8), which consist mainly of resedimented ooids (cf. Zempolich et al. 1999) (Fig. 7/3). Member 3 (m3) is of late Bathonian to early Callovian age and represents most of the proximal facies associations deposited in an upper slope environment (Šmuc 2005; Šmuc & Goričan 2005). It is composed of amalgamated debris-flow breccia beds and coarse to fine-grained calciturbidites. Breccia beds are composed of lithoclasts derived from the underlying lithologies of Members 1 and 2 and older Jurassic formations, and of skeletal debris (Fig. 7/4), while calciturbidites consist of resedimented shallow-water skeletal debris, and ooids (Figs. 4, 8). The sediments forming Member 4 (m4) were deposited in a distal-lower slope setting (Šmuc 2005; Šmuc & Goričan 2005) and consist of pelagic background sedimentation of cherty limestones, cherts and radiolarian marls (Fig. 7/5) with intercalations of fine- to very coarse-grained calciturbidites (Figs. 4, 5, 8), in which resedimented shallow-water peloids and skeletal debris predominate (Fig. 7/6). Only the lower and middle part (carbonate part) of the Member 4 were used for our statistical analysis. The age of this part of the succession is defined as Late Bathonian/Early Callovian to Middle/Late Oxfordian (Šmuc 2005; Šmuc & Goričan 2005).

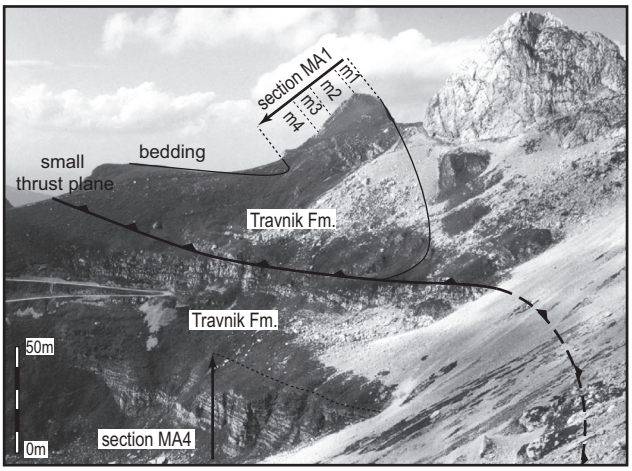

Fig. 2. View from the MA3 section on the Mt. Mangart Saddle with marked general tectonic features and sections MA1 and MA4. Note that the MA1 section is in overturned position.

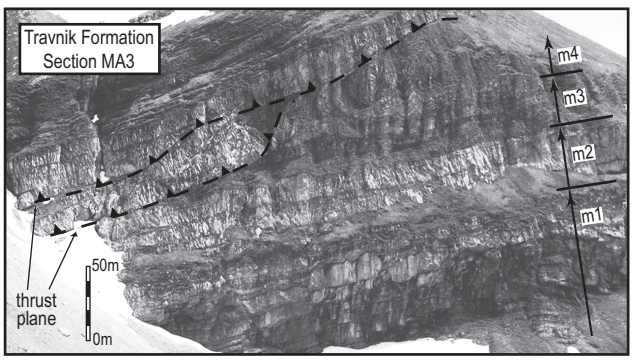

Fig. 3. View of the MA3 section with marked general tectonic features and members of the Travnik Fm.

Methods and materials

Our study is based on the Fourier analysis of the bed thicknesses in three detailed sections (MA1, MA3, MA4) revealing parts of the Travnik Formation. The present-day spatial distances (measured from the southernmost section MA3) are MA3–MA4=approx. 250 m and MA3–MA1=approx. 500 m.

For the analysis, only data sets were used that can be directly correlated in at least two sections. The member m4 is an exception, since it only exists in one section (M1). This allowed us to detect the possible variability of cyclicity and bed thicknesses within the same time frame of deposition and also to detect the subtle lateral variation of the stacking pattern between the sections.

The data set is based on very detailed sections that were measured bed by bed. For each individual bed thickness, structure and texture were recorded macroscopically. Additionally, more than 500 thin sections were made to detect the compositional variability (using Folk/Dunham classification) and to validate the macroscopic observations. Where beds of turbidites were obviously amalgamated we counted each visible bed, separated by amalgamation surfaces.

For statistical analysis we used the Statistica 8 program (Statsoft, Inc.). For quantification, we first evaluated the mean value and standard deviation to analyse the differences between the members and check the variability of their bed thicknesses and mean entire bed grain sizes. Further analyses were performed by Fourier analysis of the bed thickness data. In the calculation we used all measured beds. To obtain the information about the strength of each cycle, a value, called a periodogram, is calculated from the sine and cosine coefficients (Pk=[sine coefficient^2+cosine coefficient^2]*N/2) of each frequency or period in the series (stronger periods show stronger peaks). Periodograms are used to determine the cyclicity of data and are also useful for data recorded at irregular time intervals (Tarafdar & Harper 2008). Cycles are present if they are visible on the periodogram as peaks – high frequency cycles appear on the left side, and longer (low frequency) cycles on the right side.

Note that a value of one is not considered to be a cycle because it extends through all available data. The total thickness of all three sections used in the statistical calculations is 179.97 m, and a total of 1467 beds were measured.

A detailed correlation of all three sections (MA1, MA3, MA4) was possible as there are distinct marker beds with specific texture, structure and composition in all investigated sections (see Šmuc 2005; Šmuc & Goričan 2005).

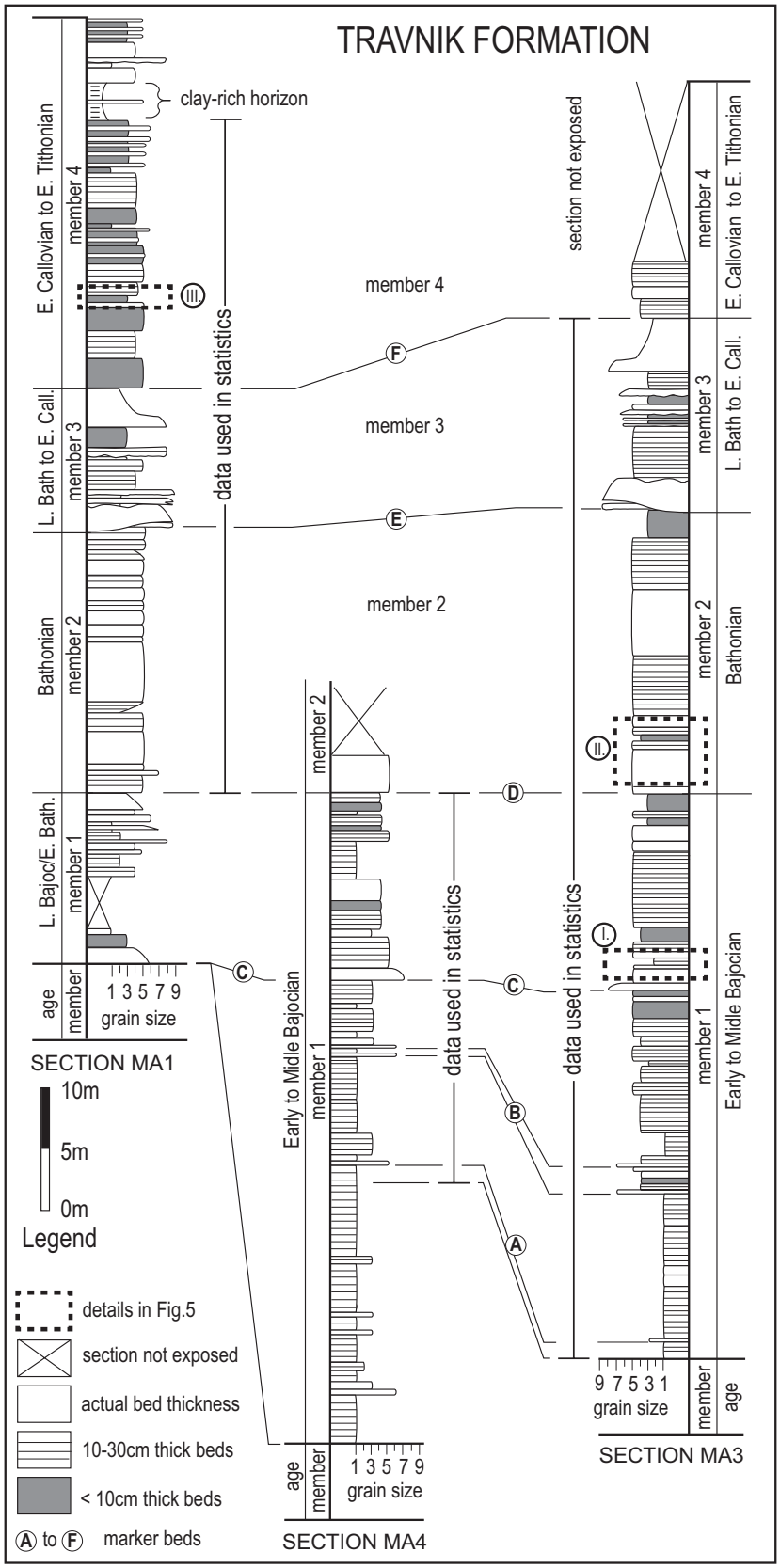

Fig. 4. Correlation of the investigated sections of the Travnik Fm. Grain size is given in classes, using the classification of McLane (1995): *class 1* = clay (<0.002 mm); *class 2* = silt (0.002–0.064 mm); *class 3* = very fine sand (0.064–0.125 mm); *class 4* = fine sand (0.125–0.25 mm); *class 5* = medium sand (0.25–0.5 mm); *class 6* = coarse sand (0.5–2 mm); *class 7* = granules (2–4 mm); *class 8* = pebbles (4–64 mm) and *class 9* = cobbles and boulders (>64 mm).

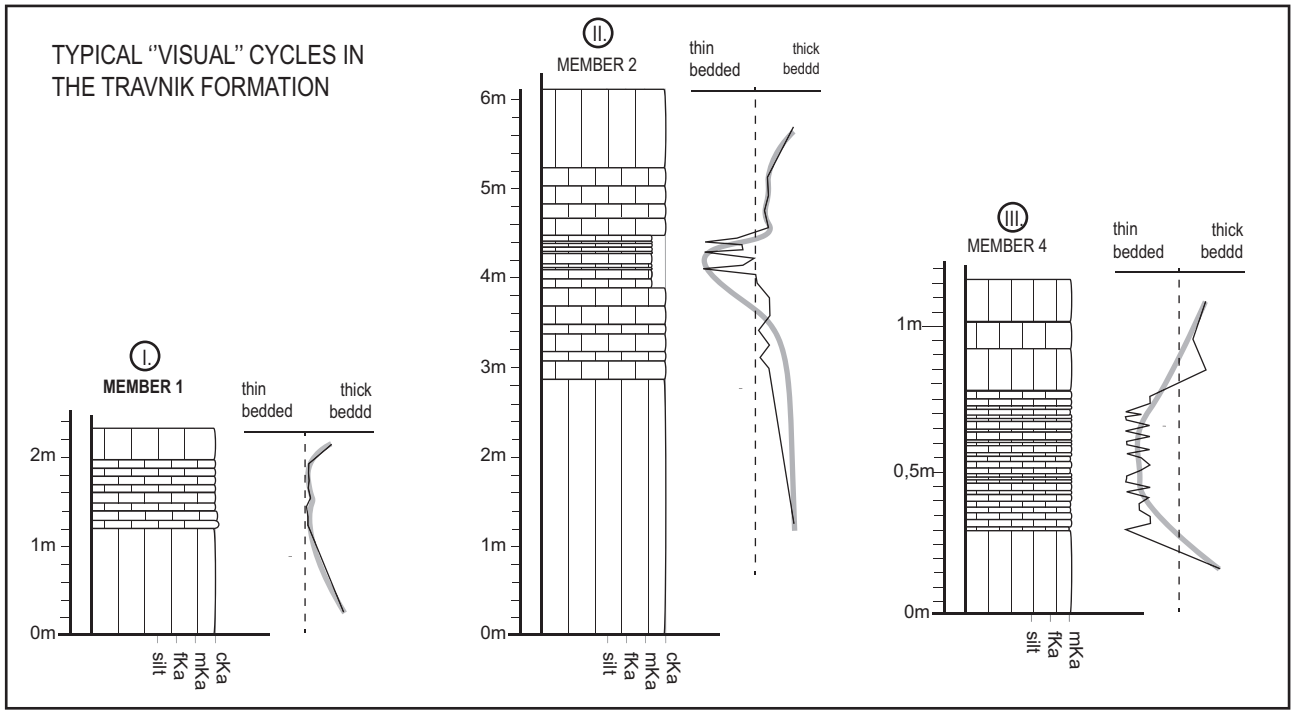

Fig. 5. Typical "visual" bed thickness cycles that occur in the individual members of the Travnik Formation, based on the variations in the bed thickness.

Fig. 6. Lower part of the MA4 section: bedded hemipelagic limestone with cherts. Scale indicated.

Results and discussion

Member 1 (m1)

Overall, Member 1 consists mainly of pelagic deposits with periplatform ooze showing a minor amount of intercalated calciturbidites (Figs. 4, 5, 7/1, 7/2, 7/3, 9) deposited in a distal deep-water environment (Šmuc 2005; Šmuc & Goričan 2005).

Periplatform ooze beds are 5 to 70 cm thick homogenous mudstone/wackestone with calcified radiolarians, and filaments (Fig. 7/1). They contain intercalated beds and lenses of replacement chert. Upwards within the member, intercalations of calciturbidite limestones occur. The calciturbidites are medium-grained packstones, beds thicken up to 20 cm and mainly exhibit horizontal lamination (Tb Bouma division), while normal grading and ripple-cross lamination rarely occur (Ta–c Bouma sequence). Grains consist of ooids, filaments, and rare peloids, echinoderm fragments, and benthic foraminifers (Fig. 7/2). One of these beds represents marker bed A (see Fig. 4). In this part of the sequence also thinner (up to 10 cm thick) and fine-grained packstone/wackestones show up. They exhibit horizontal and ripple-cross lamination, and convolute laminations (Tb–d Bouma sequences), but rarely show normal grading (Ta Bouma division). The grains are composed of partially calcified radiolarians, filaments, echinoderm

fragments and sponge spicules. In the middle part of member 1 two 10 cm thick green coarse-grained calcarenite beds are present. These are grainstones composed of abundant echinoderm grains, glauconite grains and rare mudstone intraclasts. These two coarse-grained beds represent marker beds B (Fig. 4). In the upper part of Member 1, a 1 m thick fine-grained, poorly- to medium-sorted clast-supported breccia bed occurs that grades into a thin- to medium-bedded, coarse

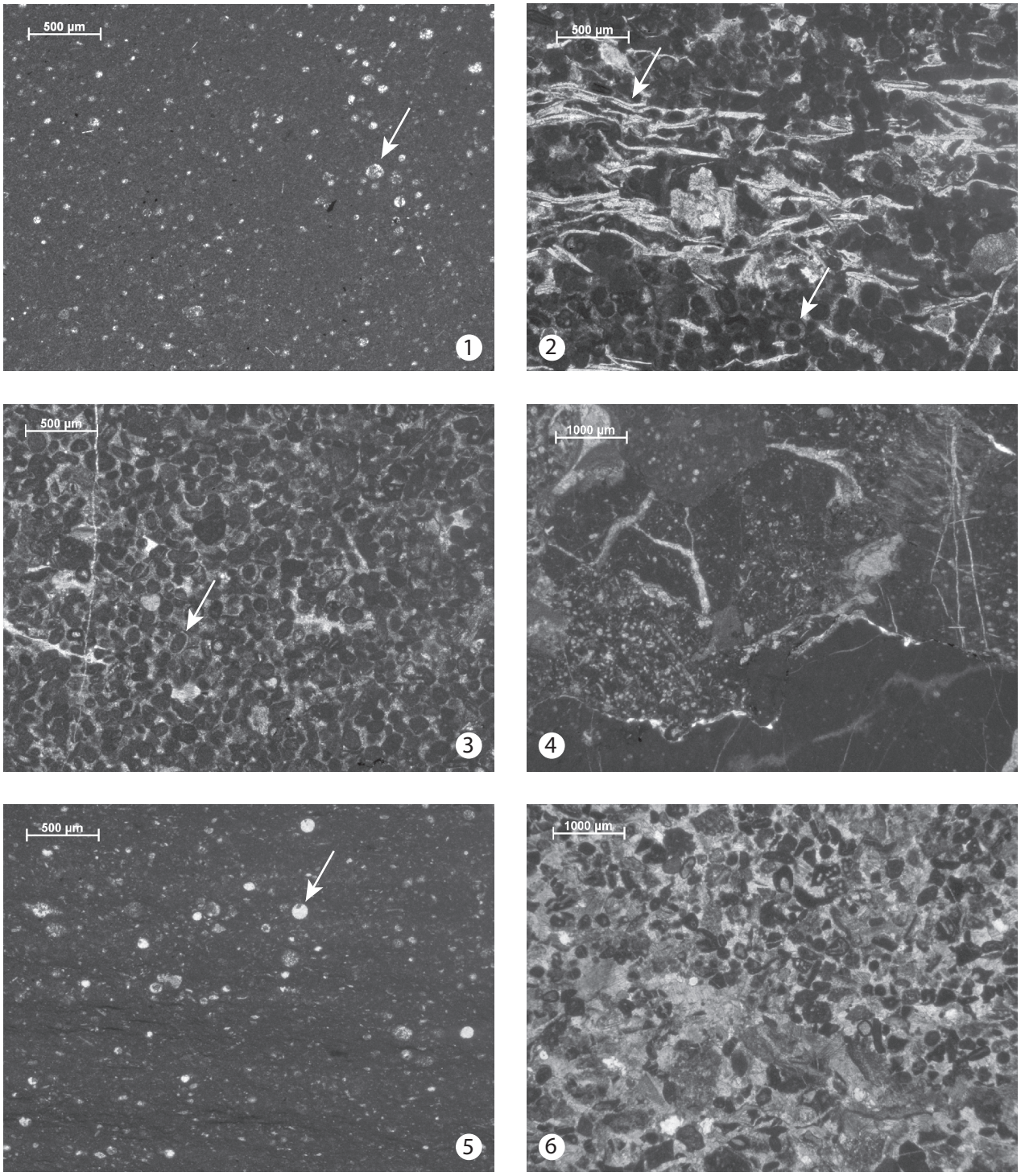

Fig. 7. 1 — Member 1. Hemipelagic wackestone with calcified radiolarian moulds (arrow). **2** — Member 1. Intercalated calciturbidites. Laminated calciturbidites: packstones with filaments (arrow) and superficial ooids (arrow). **3** — Member 2. Thick bedded calciturbidites, packstones with supperficial ooids (arrow). **4** — Member 3. Breccias. Calcirudite with lithoclasts of older Jurassic lithologies. **5** — Member 4. Pelagic laminated cherty limestone with radiolarians (arrow). **6** — Member 4. Calciturbidites with predominant echinoderm fragments, foraminifers, and sparitc bioclasts.

to medium-grained calcarenite. The breccia shows abundant lithoclasts of the underlying lithologies, but also grains of echinoderms, bivalves, and gastropods. In the upper-calcarenite part of the bed ooids and highly evolved glauconite grains (cf. Odin & Fullagar 1988) prevail over lithoclasts. These two breccia beds represent marker beds C (Fig. 4). Member 1 ends with an alternation of previously described medium-grained ooid calcarenites and thin-bedded fine-grained calciturbidites.

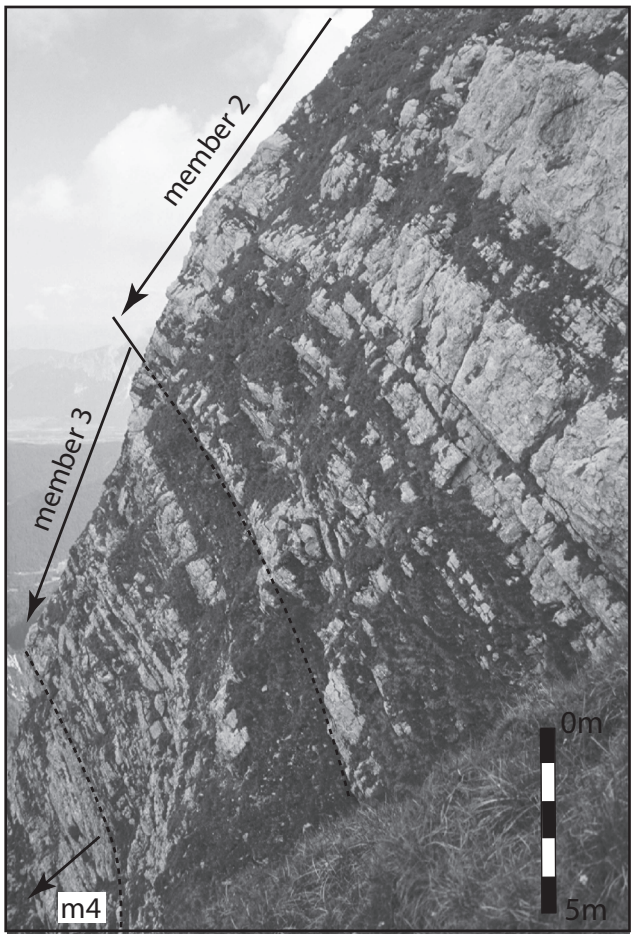

Fig. 8. Middle part of the MA1 section. Section is in overturned position.

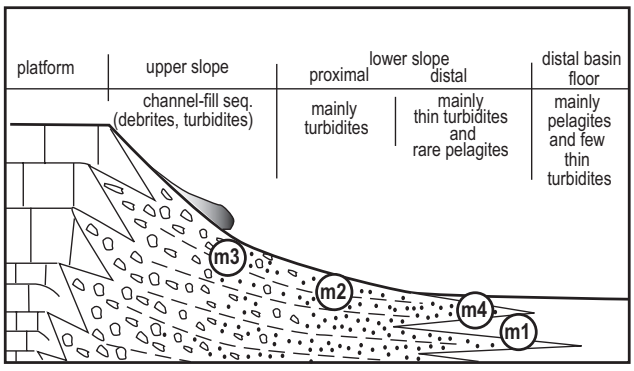

Fig. 9. The position of the Travnik investigation in a modified base-of-slope model of Mullins & Cook (1986). m1=Member 1; m2=Member 2; m3=Member 3; m4=Member 4.

Member 1 is characterized by a low mean value of bed thickness and the smallest grain size of the data in comparison to all other members (Table 1). The calculated number of present cycles within the member 1 with Fourier analysis shows that both sections (MA4 and MA3) have a cyclicity of five cycles in member 1 (Table 2, Fig. 10).

The cyclicity of five cycles is quite strong in both sections (Fig. 10). Cycles with higher frequencies, which are in the left part of each graph, are of much less strength and therefore not as significant. There are two exceptions with stronger cycles (periodogram values) in both sections – the periodogram shows that in section MA4 the strongest cyclicity appears at seven cycles and in section MA3 the strongest cyclicity is the largest cycle (one).

With the exception of the common cyclicity of five cycles, there are discrepancies between the cycle numbers in the sections. We interpret these differences as the result of the deposition of periplatform ooze and calciturbidites on a tectonically induced complex seafloor topography. Even at the scale of a few hundred metres, the seafloor geometry was most likely controlling (forcing) facies shifts and thus created subtle differences in depositional patterns (cf. Vinnels et al. 2010; Cipriani & Bottini 2019; Cipriani et al. 2019, 2020). Additionally, the differences between the cyclicity could also be attributed to the different position on the depositional lobe (cf. Mullins & Cook 1986; Payros & Pujate 2008, see discussion). There were no stronger forcing cycles on a smaller scale, as they would be considered high frequency cycles in Figure 10.

Member 2 (m2)

Member 2 mainly consists of thick-bedded coarse-grained calciturbidites composed almost exclusively of ooids and filaments (Figs. 4, 5, 7/3, 9) deposited in a lower slope environment (Šmuc 2005; Šmuc & Goričan 2005).

Member 2 is represented almost exclusively by 0.3–5 m thick beds of medium- to coarse-grained calciturbidites (Fig. 4). Thicker beds are structureless, whereas thinner (less than 0.5 m) beds at places show normal grading, horizontal and ripple-cross lamination, (Ta–c Bouma sequences). The limestones are packstones to grainstones, dominated by ooids and filaments, and rare other grains, for example, from echinoderms, peloids, foraminifers (*Textulariidae*, *Involutinidae*, *Lituolidae*), and micritic intraclasts (Fig. 7/3). Member 2 starts with very thick beds of calcarenite that represent marker beds D in the Figure 4.

Member 2 is characterized by the largest mean value of bed thickness and thus the smallest number of beds compared to all other members (see Table 1). In both sections (MA3, MA1) Member 2 also has the largest mean grain size and the smallest standard deviation of grain size (Table 1), which results from the relatively uniform grain size and composition of the original platform material, namely the ooids.

Table 1: Basic statistical parameters of the members of the Travnik Fm. N=Number of analysed data (number of beds). Total thickness represents the sum of all individual bed thicknesses in the studied section member.

	N	Mean thickness (cm)	St. dev. thickness (cm)	Total thickness (cm)	Mean grain size (-)	St. dev. grain size (-)
MA4m1	268	13.74	11.48	36.81	3.18	1.68
MA3m1	328	14.39	16.30	47.20	3.86	1.10
MA3m2	112	20.55	58.11	23.02	5.01	0.09
MA1m2	41	57.32	83.13	23.50	4.85	0.73
MA3m3	145	10.99	17.69	15.96	4.69	2.36
MA1m3	97	12.22	25.75	11.85	3.89	1.86
MA1m4	476	4.54	4.83	21.63	4.12	0.69

The Fourier analysis shows that the common cyclicity of the main cycles in both sections (MA3 and MA1) is four (Fig. 10), and this is the strongest cyclicity in section MA3 (Table 2). However, beside the one common cyclicity, high-frequency cyclicities with periods of 13, 15, 17 and 18 and one of 54 cycles are also visible on the left side of the graphs. In section MA3 they are weaker (weaker means that their periodogram strength is lower, which means lower peaks in the periodogram) than the cyclicity of four and in section MA1 they are stronger than this cyclicity. These differences between the periodograms of sections MA3 and MA1 may be due to the following factors. They can represent a consequence of the magnitude of an individual turbidite event, since the thicker turbidite events are deposited in fan shaped sedimentary bodies large enough to coalesce within the original paleo-spatial distances of about 500 m between sections. The thinner calciturbidites, however, formed much smaller, sedimentary bodies with relatively fast lateral changes and pinching out beds (cf. Maurer & Schlager 2003) and unconnected lobes, thus creating sedimentary packages that are not genetically linked. In summary, the MA3 section is characterized by thicker turbiditic events spatially widely distributed and thus dominated by low frequency (four) cycles. At the same time, section MA1 shows an association with predominantly thinner turbiditic events that were less widely distributed. In section MA3, high-frequency (17) cycles predominate, which, however, cannot be correlated over larger distances However, large (low-frequency) events still influence the overall succession but are masked by dominant small-scale events. Other explanations for the difference in depositional patterns between the sections may be related either to subtle differences in the geometry (slope, orientation, surface architecture) of the lower slopes, the presence of multiple sources of resedimented material, each operating in a slightly different mode, or to the lateral migration of depositional lobes (see chapter Facies model and cyclicity).

Table 2: The four strongest cycles in the studied profiles by Fourier analysis. Underlined values represent the strongest cycles.

	Periods	Cycles	Periodogram
MA4m1	38.29	7	2849
	53.60	<u>5</u>	1054
	134.00	2	788
	19.14	14	758
MA3m1	328.00	1	12026
	65.60	<u>5</u>	4618
	109.33	3	2572
	36.44	9	2517
MA3m2	28.00	<u>4</u>	18802
	2.07	54	14112
	7.47	15	13877
	56.00	2	7867
MA1m2	2.35	17	45913
	3.08	13	32711
	2.22	18	29695
	10.00	<u>4</u>	25919
MA3m3	144.00	1	2259
	16.00	9	1684
	9.00	16	1543
	2.62	55	1346
MA1m3	68.00	1	5226
	34.00	2	3354
	22.67	3	2842
	17.00	4	2727
MA1m4	158.67	3	973
	79.33	6	787
	52.89	9	444
	36.62	13	242

Member 3 (m3)

Member 3 consists mainly of breccia beds (debris flows) (Figs. 4, 7/4, 9) bounded by erosional surfaces representing an erosive and mixed channel-filled sequence (Šmuc 2005; Šmuc & Goričan 2005). In addition, the deposition of the individual thick coarse-grained rudstone is immediately followed by the deposition of thin-bedded fine-grained material (Fig. 11). This bed intercalation resulted in the largest standard deviation of grain size data (Table 1).

Member 3 starts with several, up to 2.60 m thick, carbonate debris flows (breccias), some of them capped by fine-grained parallel-laminated calciturbidites. The first breccia bed of member 3 represents marker bed E on Figure 4. Breccias are grain-supported, graded, and composed of up to 5 cm large lithoclasts of underlying lithologies and fragments of

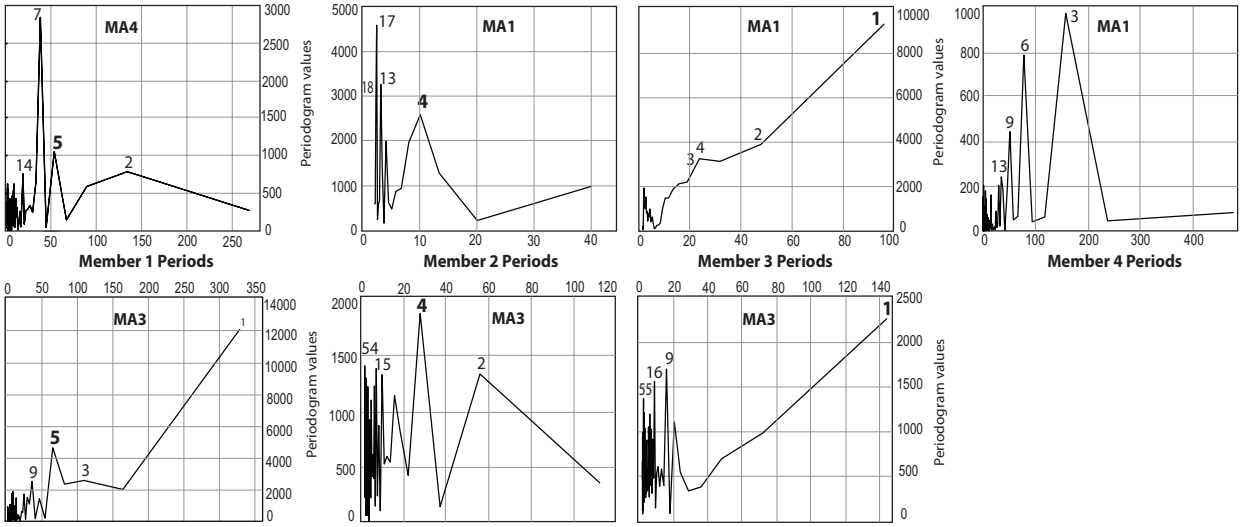

Fig. 10. Periodograms of the members of the Travnik Fm. Peaks on the curves indicate cycles, with higher peaks representing stronger cycles. Non-cyclicity is expressed as a straight line. On the left-hand side of the graphs, several small cycles appear as "noise" – very short cycles with relatively weak strength X-axis represents the period length, and Y-axis the periodogram strength values (for each corresponding period on the x-axis), calculated from sine and cosine coefficients (Pk=[sine coefficient^2+cosine coefficient^2]*N/2) Lower part of the section MA1 section: bed of coarse-graiend rudstone overlain by fine-grained calciturbidites. Erosional surface is marked with an arrow.

echinoderms, and stromatoporoids, corals and foraminifers. The overlying laminated fine-grained calciturbidites are packstone/wackestones composed of small echinoderm fragments, filaments and micritized ooids. The middle part of member 3 is dominated by thin- to medium-bedded, coarse- to fine-grained calciturbidites showing grading, parallel and ripple-cross laminations (Ta–c Bouma divisions). They have a similar composition to limestones of Member 2 but contain fewer ooids. Calciturbidites are overlain by thin-bedded partly silicified calciturbidites that exhibit horizontal, ripple-cross, and upper parallel lamination (Tb–d Bouma divisions) similar to the ones found in Member 1. Member 3 ends with a 3 m thick bed composed of a 30 cm thick breccia at the base, which abruptly passes into massive fine-grained indistinctly laminated packstone/wackestone with chert nodules (Fig. 11). The breccia has the same composition as the breccias in the lower part of Member 3. The packstone/wackestone with chert nodules series is composed of filaments, echinoderm fragments, rare ooids, phosphate grains and pyrite. This breccia bed represents marker bed F in Figure 4.

For member 3, the Fourier analysis does not show any clearly defined cycles (Table 2). For the MA1 section, the lack of cyclicity is very evident from the order of the cycles, with the cycles appearing mostly in the order from one to four. There is also no obvious peak in either section MA3 or MA1 (Fig. 10). The obvious absence of peaks applies to section MA1, and some high frequency peaks appear in section MA3 (Fig. 10). Again, there is no peak common to both sections.

This non-cyclicity can easily be explained by the depositional environment with member 3 representing an erosive and mixed channel-filled sequence (Šmuc & Goričan 2005). In such an environment, extensive erosion of older layers takes place, in addition, the coarse-grained deposits derived

Fig. 11. Lower part of the section MA1 section: bed of coarse-grained rudstone overlain by fine-grained calciturbidites. Erosional surface is marked with an arrow.

from debris flows show significant lateral thickness changes over short distances. Therefore, the preservation of the original cyclicity, due to extensive erosion and/or bypassing of previously deposited sediments is almost impossible.

Member 4 (m4)

The sediments forming member 4 consist of both pelagic background sedimentation and gravity flows which indicate deposition in a distal apron environment (Fig. 9) (Šmuc 2005; Šmuc & Goričan 2005). The lower and middle part of Member 4 that were used for our statistical analysis are characterized by thin-bedded parallel laminated (Td) black cherts and cherty limestones (same composition as cherty limestones of Member 3) with intercalated thin-bedded, fine to coarse-grained calciturbidites exhibiting grading, plane parallel, ripple-cross, and upper parallel laminations Ta–b and Tb–d Bouma divisions. The calcarenites are packstones with filaments, peloids, echinoderm fragments, benthic foraminifers, phosphate grains and rare ooids. In the coarse-grained facies, reworked lithoclasts of Member 1, 2, and 3 are present.

The average bed thickness of this member is much smaller than that of the others (Table 1), which confirms its association with a relatively distal environment. The Fourier analysis shows that the highest number of cycles is three, followed by its multiples, six and nine (Table 2), which could represent harmonic repetitions of the same cycle. No other major peaks are visible (Fig. 10). Some cycles of three thus exists for this member, but cannot be correlated because this member only appears in the MA3 section.

Facies model and cyclicity

Based on its overall sedimentary characteristics the Travnik Formation corresponds to either a medium grained, medium sized calciclastic submarine fan as defined by Pyros & Pujalte (2008) or to the base-of-slope apron model of Mullins & Cook (1986) (Fig. 9). In the first case, the members of the Travnik Formation correspond well with the outer (Member 1, Member 4), middle (Member 2), and inner (Member 3) fan environment. In this scenario the fans are sourced from unrimmed carbonate shelves or distally steepened ramps with grainy (in our case bioclastic and ooidal) accumulations. High-energy storms, tides and/or longshore drift currents transported the shallow water material from the shallow-water environments towards the slope. The sediments migrate downward via a channelized feeder system of downslope coalescing gullies first into a channel-levee system at the base of the slope and then into a system of unconfined lobe-sheets located basinward from the base of the slope (cf. Savary & Ferry 2004; Pyros & Pujalte 2008). In the case of the base-of-slope apron model, the shallow water material is shed into the basin from the line source, bypasses the upper slope and is deposited in the lower-slope apron (Mullins & Cook 1986) see also Mulder et al. 2012a,b). According to this model the members correspond to distal lower slope (Members 1 and 4), lower slope (Member 2) and upper slope channel (Member 3) environments (Fig. 9). The vertical organization of talus lobes reflect the evolution of the submarine gullies that transport material from the upper slope to the lower slope (Mullins & Cook 1986). In both cases the changes from distal to proximal and back can be controlled either by eustatic changes of sea level, tectonics and autocyclic processes, namely shifting lobes and depo-centres. These changes effect not only the quantity, quality and spatial distribution of shallow-water carbonate production, but also the processes that redistribute sediment to deeper-water environments as is clearly also indicated by work on Late Pleistocene and recent slope sediments and evolution around the Bahamas (Mulder et al. 2012a,b, 2017, 2019; Tournadour et al. 2017; Recouvreur et al. 2020) and also on the Great Barrier Reef (Puga-Bernabéu et al. 2011, 2013; Webster et al. 2012)

The age of the overall Travnik Formation and individual members was determined on the basis of well-preserved radiolarians (Šmuc 2005; Šmuc & Goričan 2005). However, an exact estimation of the age and duration of the detected cycles is not possible for the following reasons. Firstly, the investigated sections were dated using radiolarian Unitary Association Zones (UAZs), which have relatively long-time ranges and insufficient calibration to radiometric dates (Baumgartner et al. 1995). Secondly, the middle to late Jurassic period is not sufficiently constrained by radiometric data (Cohen et al. 2020), since the estimated uncertainty in the duration of the Jurassic stages is generally in the range of more than one million years. Erosion of former sedimented beds poses a problematic fact for the interpretation of cyclicity, as larger thick sections can be removed and the thicknesses are disturbed. Nevertheless, the comparison with the latest published Jurassic sea-level variations of third order by Haq (2017) and considering the long-time ranges of UAZs shows a relative good match. Haq (2017) defined seven cycles during the Bajocian and Bathonian, while our number of cycles is nine for age correlative Members 1 and 2 of the Travnik Formation. For the Early Callovian to Middle/Late Oxfordian Haq (2017) defined nine cycles and the same number of cycles also appears in age correlative Member 4 of the Travnik Formation. Due to the erosional and bypass nature of the Member 3 sedimentary environment, reliable comparison to Jurassic sea-level variations was not possible.

Conclusions

Our study has shown that the Fourier analysis of bed thicknesses of calciturbidites gives meaningful results, which can be explained in the context of the depositional environment. The method also avoids the pitfalls of a subjective visual approach of bed thickness variation determination by providing a numerical evaluation of bed thickness cycle determination in the analysed sections.

Variability of cyclicity in the same time frame of deposition and subtle lateral variation of the stacking pattern between

different sections clearly exist. Each individual section contains specific "local" high-frequency cyclicity and also overlapping low-frequency cycles common to all sections.

Tectonic factors and eustatic sea-level changes could have a lower-frequency influence (seen as strong peaks on the right-hand side of periodograms), and other factors (shifting lobes, shifting depo centres, local topography or magnitude of a turbidite event for example) can influence the high-frequency cycles (seen as peaks on the left-hand side of periodograms). The low-frequency signals are well preserved in all of the investigated sections deposited in the same time frame of deposition, while high-frequency cycles strongly vary between the aforementioned sections. High frequency cycles are not so important as low frequency ones, because they cannot be easily correlated across the sections due to the fact that they are not driven by some regional factor (tectonics, larger changes of sea level, etc., which affect several sections), but by not so intensive processes, which are shorter in time and do not have such an effect on the bed thickness distributions. Consequently, the cyclicity cannot be studied in one section only, but must be analysed at least in two sections (the more the better). The study of cyclicity in only one section without correlation can therefore cause serious inaccuracy especially if the driving factor for the cyclicity is later attributed to global events like eustasy. Fourier analysis can provide any possible output and can be quite sensitive, especially in the case of a low number of studied data (number of beds), so cycles with no reasonable geological interpretation can be falsely recognized exhibiting similar strength as those which have more sound explanation. Observation of the same cycle in more sections helps us to recognize the 'true' cycles and distinguish them from the others.

We also show that Fourier analysis of bed thicknesses of calciturbidites shows good agreement with the latest published Jurassic third-order sea level variations of Haq (2017).

Acknowledgements: The authors thank André Strasser and an anonymous reviewer for thorough review and constructive comments that improved this paper. This work was supported by the Slovenian Research Agency within the research programme P1-0195 (Geo-environment and Geomaterials).

References

Andresen N., Reijmer J.J.G. & Droxler A.W. 2003: Timing and distribution of calciturbidites around a deeply submerged carbonate platform in a seismically active setting (Pedro Bank, Northern Nicaragua Rise, Caribbean Sea). *International Journal of Earth Sciences* 92, 573–592. https://doi.org/10.1007/s00531-003-0340-0

Anselmetti F., Eberli G.P. & Ding D-Z. 2000: From Great Bahama Bank into the Straits of Florida: Margin architecture controlled by sea-level fluctuations and ocean currents. *GSA Bull*etin 112, 829–844. https://doi.org/10.1130/0016-7606(2000)112%3C829:FTGBBI%3E2.0.CO;2

Baumgartner P.O., Bartolini A., Carter E.S., Conti M., Cortese G., Danelian T., Wever P.D., Dumitrica P., Dumitrica-Jud R., Goričan Š., Guex J., Hull, D.M., Kito N., Marcucci M., Matsuoka A., Murchey B., O'Dogerthy L., Savary J., Vishnevskaya V., Widz D. & Yao A. 1995: Middle Jurassic to Early Cretaceous radiolarian biochronology of Tethys based on Unitary Associations. In: Baumgartner P.O., O'Dogerthy L., Goričan Š., Urquhart E., Pillevuit A. & Wever P.D. (Eds.): Middle Jurassic to Lower Cretaceous Radiolaria of Tethys: Occurrences, Systematics, Biochronology. *Mémoires de Géologie* 23, 1013–1038.

Bernet K.H., Eberli G.P. & Gilli A. 2000: Turbidite Frequency and composition in the distal part of the Bahamas transect. In: Swart P.K., Eberli G.P., Malone M.J. & Sarg J.F. (Eds.): P*roceedings of the Ocean Drilling Program, Scientific Results* 166, 45–60. https://doi.org/10.2973/odp.proc.sr.166.105.2000

Betzler C., Brachert T.C. & Kroon D. 1995: Role of climate in partial drowning of the Queensland plateau carbonate platform (northeastern Australia). *Marine Geology* 123, 11–32. https://doi.org/10.1016/0025-3227(95)80002-S

Betzler C., Reijmer J.J.G., Bernet K., Eberli G.P. & Anselmetti F. 1999: Sedimentary patterns and geometries of the Bahamian outer carbonate ramp (Miocene-Lower Pliocene, Great Bahama Bank). *Sedimentology* 46, 1127–1143. https://doi.org/10.1046/j.1365-3091.1999.00268.x

Betzler C., Pfeiffer M. & Saxena S. 2000: Carbonate shedding and sedimentary cyclicities of a distally steepened carbonate ramp (Miocene, Great Bahama Bank). *Geologische Rundschau* 89, 140–153. https://doi.org/10.1007/s005310050322

Blomeier D.P.G. & Reijmer J.J.G. 2002: Facies architecture of and Early Jurassic carbonate platform slope (Jbel Bou Dahar, High Atlas, Morocco). *Journal of Sedimentary Research* 72, 462–475. https://doi.org/10.1306/111501720462

Bosence D., Procter E., Aurell M., Bel Kahla A., Boudagher-Fadel M., Casaglia F., Cirilli S., Mehdie M., Nieto L., Rey J., Scherreiks R., Soussi M. & Waltham D. 2009: A dominant tectonic signal in high-frequency, peritidal carbonate cycles? A regional analysis of Liassic Platforms from Western Tethys. *Journal of Sedimentary Research* 79, 389–415. https://doi.org/10.2110/jsr.2009.038

Buser S. 1989: Development of the Dinaric and the Julian Carbonate Platforms and of the intermediate Slovenian Basin (NW Yugoslavia). *Memorie della Societa Geologica Italiana* 40, 313–320.

Cipriani A. & Bottini C. 2019: Unconoformities, neptunian dykes and mass-transport depostis as an evidence for Early Cretaceous syn-sedimetnary tectonics: new insights from the Central Apennines. *Italian Journal of Geosceines* 138, 333–354. https://doi.org/10.3301/IJG.2019.09

Cipriani A., Caratelli M. & Santantonio M. 2019: Geological mapping reveals the role of Early Jurassic rift architecture in the dispersal of calciturbidites: new insights from the Central and Northern Apennines. *Mendeley Data* V2. https://doi.org/10.17632/5j66smvyzf.2

Cipriani A., Caratelli M. & Santantonio M. 2020: Geological mapping reveals the role of Early Jurassic rift architecture in the dispersal of calciturbidites: New insights from Central and Norhern Apennines. *Basin Research* 32, 1485–1509. https://doi.org/10.1111/bre.12438

Cohen K.M., Finney S.C., Gibbard P.L. & Fan J.-X. (2013; updated): The ICS International Chronostratigraphic Chart. *Episodes* 36, 199–204. https://doi.org/10.18814/epiiugs/2013/v36i3/002

Cousin M. 1981: Les rapports Alpes-Dinarides. Les confines de l'Italie e de la Yugoslavie. *Société Géologique du Nord.* 5, 1–521.

Črne A.E., Šmuc A. & Skaberne D. 2007: Jurassic neptunian dikes at Mt Mangart (Julian Alps, NW Slovenia). *Facies* 53, 2249–265.

D'Argenio B., Ferreri V., Raspini A., Amodio S. & Buoncounto F.P. 1999: Cyclostratigraphy of a carbonate platform as a tool for high-precision correlation. *Tectonophysics* 315, 357–384. https://doi.org/10.1016/S0040-1951(99)00290-5

Drzewiecki P.S. & Simo J.A. 2002: Depositional processes, triggering mechanisms and sediment composition of carbonate gravity flow deposits: examples from the Late Cretaceous of the south-central Pyrenees, Spain. *Sedimentary Geology* 146, 155–189. https://doi.org/10.1016/S0037-0738(01)00171-3

Eberli G.P. 1991: Calcareous Turbidites and Their Relationship to Sea-Level Fluctuations and Tectonism. In: Einsele G., Richen W. & Seilacher A. (Eds.): Cycles and Events in Stratigraphy. *Springer-Verlag*, 340–359.

Everts J.W. 1991: Interpreting compositional variations of calciturbidites in relation to platform stratigraphy: an example from the Paleogene of SE Spain. *Sedimentary Geology* 71, 231–242.

Everts J.W., Schlager W. & Reijmer J.J.G. 1999: Carbonate to platform-to-basin correlation by means of grain-composition logs: and example the Vercors (Cretaceous, SE France). *Sedimentology* 46, 261–278.

Ferry S. & Rubino J.-L. 1987: Les séquences carbonatées nécomiennes du Sud-Est de la France sont-elles le résultat d´oscillations eustatiques? *Comptes rendus de l'Académie des Sciences – Géologie* 304, 917–922.

Goričan Š., Šmuc A. & Baumgartner P.O. 2003: Toarcian Radiolaria from Mt. Mangart (Slovenian–Italian border) and their paleoecological implication. *Marine micropaleontology* 932, 1–27. https://doi.org/10.1016/S0377-8398(03)00034-3

Haak A.B. & Schlager W. 1989: Compositional variations in calciturbidites due to sea-level fluctuations, late Quaternary, Bahamas. *Geologische Rundschau* 78, 477–486.

Haq B.U. 2017: Jurassic sea-level variations: A reapraisal. *GSA Today* 28, 4–10. https://doi.org/10.1130/GSATG359A.1

Isern A.R. & Anselmetti F. 2001: The influence of carbonate platform morphology and sea level on fifth-order petrophysical cyclicity in slope and basin sediments adjacent to the Great Bahama Bank. *Marine Geology* 177, 381–394. https://doi.org/10.1016/S0025-3227(01)00154-2

Jurkovšek B., Šribar L., Ogorelec B. &Kolar-Jurkovšek T. 1990: Pelagic Jurassic and Cretaceous beds in the western part of the Julian Alps. *Geologija* 31–32, 285–328.

Lantzsch H., Roth S., Reijmer J.J.G. & Kinkel H. 2007: Sea-level related resedimentation processes on the northern slope of Little Bahama Bank (Middle Pleistocene to Holocene). *Sedimentology* 54, 1307–1322. https://doi.org/10.1111/j.1365-3091.2007.00882.x

Maurer F. & Schlager W. 2003: Lateral variations in sediment composition and bedding in Middle Triassic interplatform basins (Buchenstein Formation, southern Alps, Italy). *Sedimentology* 50, 1–22. https://doi.org/10.1046/j.1365-3091.2003.00499.x

Maurer F., Reijmer J.J.G. & Schlager W. 2003: Quantification of input and compositional variations of calciturbidites in a Middle Triassic basinal succession (Seceda, Dolomites, Southern Alps). *International Journal of Earth Sciences* 92, 593–609.

Mawson M. & Tucker M. 2009: High-frequency cyclicity (Milankovitch and millennial-scale) in slope-apron carbonates: Zechstein (Upper Permian), North-east England. *Sedimentology* 56, 1905–1936. https://doi.org/10.1111/j.1365-3091.2009.01062.x

McLane M. 1995: Sedimentology. *Oxford University Press*, New York, 1–423.

Mulder T., Ducassou E., Eberli G.P., Hanquiez V., Gonthier E., Kindler P., Principaud M., Fournier F., Léonide P., Billeaud I., Marsset B., Reijmer J.J.G., Bondu C., Joussiaume R. & Pakiades M. 2012a: New insights into the morphology and sedimentary processes along the western slope of Great Bahama Bank. *Geology* 40, 603–606. https://doi.org/10.1130/G32972.1

Mulder T., Ducassou E., Gillet H., Hanquiez V., Tournadour E., Combes J., Eberli G.P., Kindler P., Gonthier E., Conesa G., Robin C., Sianipar R., Reijmer J.J.G. & Francois A. 2012b: Canyon morphology on a modern carbonate slope of the Bahamas: Evidence of regional tectonic tilting. *Geology* 40, 771–774. https://doi.org/10.1130/G33327.1

Mulder T., Gillet H., Hanquiez V., Ducassou E., Fauquembergue K., Principaud M., Conesa G., Le Goff J., Ragusa J., Bashah S., Bujan S., Reijmer J.J.G., Cavailhes T., Droxler A.W., Blank D.G., Guiastrennec L., Fabregas N., Recouvreur A. & Seibert C. 2017: Carbonate slope morphology revealing a giant submarine canyon (Little Bahama Bank, Bahamas). *Geology*, 46, 31–34. https://doi.org/10.1130/G39527.1

Mulder T., Gillet H., Hanquiez V., Reijmer J.J.G., Droxler A.W., Recouvreur A., Fabregas N., Cavailhes T., Fauquembergue K., Blank D.G., Guiastrennec L., Seibert C., Bashah S., Bujan S., Ducassou E., Principaud M., Conesa G., Le Goff J., Ragusa J., Busson J. & Borgomano J. 2019: Into the deep: A coarse-grained carbonate turbidite valley and canyon in ultra-deep carbonate setting. *Marine Geology* 407, 316–333. https://doi.org/10.1016/j.margeo.2018.11.003

Mullins H.T. & Cook H.E. 1986: Carbonate Apron Models: Alternatives to the Submarine Fan Model for Paleoenvironmental Analysis and Hydrocarbon Exploration. *Sedimentary Geology* 48, 37–79.

Nicolis G. & Nicolis C. 1991: Nonlinear dynamic systems in the geosciences. In: Franseen E.K., Watney W.L., Kendall C.G.St.C., & Ross W. (Eds.): Sedimentary Modeling: Computer simulation and Method for Improved Parameter Definition. *Kansas Geological Survey Bulletin* 233, 33–42.

Odin G.S.& Fullagar P.D. 1988: Geological significance of the Glauconi facies. In: Odin G.S. (Ed.): Green Marine Clays. *Developments in Sedimentology* 45, 295–332. https://doi.org/10.1016/S0070-4571(08)70069-4

Payros A. & Pujalte V. 2008: Calciclastic submarine fans: An integrated overview. *Earth-Science Reviews* 86, 203–246. https://doi.org/10.1016/j.earscirev.2007.09.001

Placer L. 2008: Principles of the tectonic subdivision of Slovenia. *Geologija* 51, 205–217.

Puga-Bernabéu Á., Webster J.M., Beaman R.J. & Guilbaud V. 2011: Morphology and controls on the evolution of a mixed carbonate–siliciclastic submarine canyon system, Great Barrier Reef margin, north-eastern Australia. *Marine Geology* 289, 100–116. https://doi.org/10.1016/j.margeo.2011.09.013

Puga-Bernabéu Á., Webster J.M., Beaman R.J. & Guilbaud V. 2013: Variation in canyon morphology on the Great Barrier Reef margin, north-eastern Australia: The influence of slope and barrier reefs. *Geomorphology* 191, 35–50. https://doi.org/10.1016/j.geomorph.2013.03.001

Recouvreur A., Fabregas N., Mulder T. Hanquiez V. Fauquembergue K., Tournadour E., Gillet H., Borgomano J., Poli E., Kucharski J.-B. & Wilk S. 2020: Geomorphology of a modern carbonate slope system and associated sedimentary processes: Example of the giant Great Abaco Canyon, Bahamas. *Sedimentology*, early view. https://doi.org/10.1111/sed.12777

Reijmer J.J.G. 1998: Compositional variations during phases of progradation and retrogradation of a Triassic carbonate platform (Picco di Vallandro/Dürrenstein, Dolomites, Italy). *Geologische Rundschau* 87, 436–448. https://doi.org/10.1007/PL00009941

Reijmer J.J.G. & Everaars J.S.L. 1991: Carbonate platform facies reflected in carbonate basin facies (Triassic, Northern Calcareous Alps, Austria). *Facies* 25, 253–277. https://doi.org/10.1007/BF02536761

Reijmer J.J.G., Schlager W. & Droxler A. 1988: ODP Site 632: Pliocene-Pleistocene sedimentation cycles in a Bahamian basin. In: Austin J.A., Schlager W. et al. (Eds.): Proceedings of the Ocean Drilling Program, Scientific Results. Texas, 213–220.

Reijmer J.J.G., Ten Kate W.G.H.Z., Sprenger A. & Schlager W. 1991: Calciturbidite composition related to the exposure and flooding

of a carbonate platform (Triassic, Eastern Alps). *Sedimentology* 38, 1059–1074. https://doi.org/10.1111/j.1365-3091.1991.tb00371.x

Reijmer J.J.G., Schlager W., Bosscher, H. Beets C.J. & McNeill D.F. 1992: Pliocene/Pleistocene platform facies transition recorded in calciturbidites (Exuma Sound, Bahamas). *Sedimentary Geology Expressed* 78, 171–179.

Reijmer J.J.G., Sprenger A., Ten Kate, W.G.H.Z., Schlager W. & Krystyn L. 1994: Periodicities in the composition of Late Triassic calciturbidites (Eastern Alps, Austria). In: De Boer P.L. & Smith D.G. (Eds.): Orbital forcing and cyclic sequences. *Special Publication of the International Association of Sedimentologists* 19, 323–343.

Reijmer J.J.G., Palmieri P. & Groen R. 2012: Compositional variations in calciturbidites and calcidebrites in response to sea-level fluctuations (Exuma Sound, Bahamas). *Facies* 58, 493–507. https://doi.org/10.1007/s10347-011-0291-z

Reijmer J.J.G., Palmieri P., Groen R. & Floquet M. 2015: Calciturbidites and calcidebrites: Sea-level variations or tectonic processes? *Sedimentary Geology* 317, 53–70. https://doi.org/10.1016/j.sedgeo.2014.10.013

Rendle R.H & Reijmer J.J.G. 2002: Quarternary slope development of the western, leeward margin of the Great Bahama Bank. *Marine Geology* 185, 143–164. https://doi.org/10.1016/S0025-3227(01)00294-8

Roth S. & Reijmer J.J.G. 2005: Holocene millennial to centennial carbonate cyclicity recorded in slope sediments of the Great Bahama Bank and its climatic implications. *Sedimentology* 52, 161–181. https://doi.org/10.1111/j.1365-3091.2004.00684.x

Satterley A.K. 1996: The interpretation of cyclic successions of the Middle and Upper Triassic of the Northern and Southern Alps. *Earth-Science Reviews* 20, 181–207. https://doi.org/10.1016/0012-8252(95)00063-1

Savary B. & Ferry S. 2004: Geometry and petrophysical parameters of a calcarenitic turbidite lobe (Barremian–Aptian, Pas-de-la-Cluse, France). *Sedimentary Geology* 168, 281–304. https://doi.org/10.1016/j.sedgeo.2004.04.004

Schwarzacher W. 2000: Repetitions and cycles in stratigraphy. *Earth-Science Reviews* 50, 51–75. https://doi.org/10.1016/S0012-8252(99)00070-7

Šmuc A. 2005: Jurassic and Cretaceous stratigraphy and sedimentary evolution of the Julian Alps, NW Slovenia. *Založba ZRC Publishing*, Ljubljana, 1–98.

Šmuc A. & Goričan Š. 2005: Jurassic sedimentary evolution from carbonate to deeper-water basin: a succession at Mt Mangart (Slovenian-Italian border). *Rivista Italiana di Paleontologia e Stratigrafia* 111, 45–70. https://doi.org/10.13130/2039-4942/6269

Tarafdar S. & Harper D. 2008: Anti-persistence in levels of Lake Naivasha: Assessing effect of human intervention through time-series analysis. *Physica A: Statistical Mechanics and its Applications* 387, 296–302. https://doi.org/10.1016/j.physa.2007.08.050

Tresch J. & Strasser A. 2011: Allogenic and autogenic processed combined in the formation of shallow-water carbonate sequences (Middle Berriasian, Swiss and French Jura Mountains). *Swiss Journal of Geosciences* 104, 299–322. https://doi.org/10.1007/s00015-011-0064-2

Tournadour E., Mulder T., Borgomano J., Gillet H., Chabaud L., Ducassou E., Hanquiez V. & Etienne S. 2017: Submarine canyon morphologies and evolution in modern carbonate settings: The northern slope of Little Bahama Bank, Bahamas. *Marine Geology* 391, 76–97. https://doi.org/10.1016/j.margeo.2017.07.014

Vinnels J.S., Butler R.W.H., McCaffrey W.D. & Lickorish W.H. 2010: Sediment distribution and architecture around a bathymetrically complex basin: an example from the eastern Champsaur Basin, SE France. *Journal of Sedimentary Research* 80, 216–235.

Webster J.M., Beaman R.J., Puga-Bernabéu Å., Ludman D., Renema W., Wust R.A.J., George N.P.J., Reijmer P.J., Jacobsen G.E. & Moss P. 2012: Late Pleistocene history of turbidite sedimentation in a submarine canyon off the northern Great Barrier Reef, Australia. *Palaeogeography, Palaeoclimatology, Palaeoecology* 331–332, 75–89. https://doi.org/10.1016/j.palaeo.2012.02.034

Zempolich W.G. & Erba E. 1999: Sedimentologic and chemostratigraphic recognition of third-order sequences in resedimented carbonate: The Middle Jurassic Vajont Limestone, Venetian Alps, Italy. In: Harris P.M., Saller A.H. & Simo J.A. (Eds.): Advances in carbonate sequence stratigraphy: Application to reservoirs, outcrops and models. *SEPM Special Publication* 63, 335–370. https://doi.org/10.2110/pec.99.11.0335v